NASA TECHNICAL NOTE

NASA TN D-2829

TRANSONIC AERODYNAMIC CHARACTERISTICS OF A SATURN IB-APOLLO LAUNCH VEHICLE WITH VARIOUS UPPER-STAGE CONFIGURATIONS

by C. Robert Carter

Langley Research Center
Langley Station, Hampton, Va.

NATIONAL AERONAUTICS AND SPACE ADMINISTRATION • WASHINGTON, D. C. • JUNE 1965

TRANSONIC AERODYNAMIC CHARACTERISTICS OF A

SATURN IB-APOLLO LAUNCH VEHICLE WITH

VARIOUS UPPER-STAGE CONFIGURATIONS

By C. Robert Carter

Langley Research Center
Langley Station, Hampton, Va.

TRANSONIC AERODYNAMIC CHARACTERISTICS OF A

SATURN IB-APOLLO LAUNCH VEHICLE WITH

VARIOUS UPPER-STAGE CONFIGURATIONS

By C. Robert Carter
Langley Research Center

SUMMARY

25547

A wind-tunnel investigation has been conducted in the Langley 8-foot tran-
sonic pressure tunnel to determine the transonic aerodynamic characteristics of
the Saturn IB-Apollo launch vehicle with various upper-stage configurations.
The tests were conducted at Mach numbers from 0.50 to 1.20, angles of attack
from $-6°$ to $18°$, angles of sideslip from $-4°$ to $10°$, and Reynolds number per
foot from 2.76×10^6 to 4.22×10^6.

The results of this investigation indicate that the normal-force contribu-
tion of the fins was approximately 50 percent of the total normal force acting
on the entire vehicle. The abort configuration showed a substantial increase
in axial force over the other configurations tested; however, the differences
in force and moment coefficients were generally small for all configurations.
Also, removal of the protuberances from the second stage (S-IV-B) had a greater
effect on the normal-force and pitching-moment characteristics, as compared
with the basic configuration, than did increasing the angle of the forward
flare.

INTRODUCTION

The National Aeronautics and Space Administration is currently conducting
a program to define the geometry of the Saturn IB launch vehicles with an Apollo
payload. As a part of this program, tests were conducted at subsonic and tran-
sonic speeds in the Langley 8-foot transonic pressure tunnel. The launch con-
figurations were simulated by the use of interchangeable upper-stage configura-
tions on the basic launch vehicle.

The longitudinal, and limited lateral, aerodynamic characteristics of the
Saturn IB with various upper-stage payload combinations were investigated as a
part of an evaluation program to determine the most suitable launch vehicle.
These experimental data were needed for trajectory and control evaluation
through the critical transonic speed range. Even though the transient time of
a vehicle through the transonic speed range is generally relatively short, the
transonic aerodynamic characteristics (particularly the drag) may influence the

general timing of the events of the launch trajectory. In this regard, wind-tunnel data are required in simulation studies needed as an aid in the early determination of nominal trajectories.

The investigation was conducted at Mach numbers from 0.50 to 1.20, angles of attack from -6° to 18°, and angles of sideslip from -4° to 10°. The Reynolds number per foot varied from 2.76×10^6 to 4.22×10^6.

SYMBOLS

The forces and moments measured on the vehicle were referred to the body system of coordinate axes with the origin located at the engine gimbal station 100 (0.607 inch forward of the base, model scale), as shown in figure 1. The coefficients and symbols used herein are defined as follows:

A   reference area (across tanks) of 1.32-percent-scale model of Saturn IB launch vehicle, 0.0627 sq ft

C_N normal-force coefficient, $\dfrac{\text{Normal force}}{qA}$

C_A axial-force coefficient, $\dfrac{\text{Axial force}}{qA}$

$C_{A,\alpha=0^\circ}$ axial-force coefficient at $\alpha = 0^\circ$

$C_{A,b}$ base axial-force coefficient, $\dfrac{\text{Base axial force}}{qA}$

C_m pitching-moment coefficient, $\dfrac{\text{Pitching moment}}{qAd}$

C_l rolling-moment coefficient, $\dfrac{\text{Rolling moment}}{qAd}$

C_n yawing-moment coefficient, $\dfrac{\text{Yawing moment}}{qAd}$

C_Y side-force coefficient, $\dfrac{\text{Side force}}{qA}$

C_{N_α} normal-force-curve slope at $\alpha = 0^\circ$, $\dfrac{\partial C_N}{\partial \alpha}$, per deg

C_{m_α} pitching-moment curve slope at $\alpha = 0^\circ$, $\dfrac{\partial C_m}{\partial \alpha}$, per deg

C_{n_β} yawing-moment-curve slope at $\beta = 0^\circ$, $\dfrac{\partial C_n}{\partial \beta}$, per deg

C_{p_b} base pressure coefficient, $\dfrac{p_b - p}{q}$

C_{Y_β} side-force-curve slope at $\beta = 0^\circ$, $\dfrac{\partial C_Y}{\partial \beta}$, per deg

d reference diameter (across tanks) of 1.32-percent-scale model of Saturn IB launch vehicle, 0.2827 ft

D diameter

M free-stream Mach number

p free-stream static pressure, lb/sq ft

p_b static pressure at model base, lb/sq ft

q free-stream dynamic pressure, lb/sq ft

R radius

S_b base area (shroud area included) of 1.32-percent-scale model of Saturn IB launch vehicle, 0.0777 ft^2

$\dfrac{x_{cp}}{d}$ location of center of pressure in body diameters forward of engine gimbal station 100 at $\alpha = 0^\circ$, $\dfrac{C_{m_\alpha}}{C_{N_\alpha}}$

α angle of attack, deg

β angle of sideslip, deg

APPARATUS AND TESTS

Tunnel

The Langley 8-foot transonic pressure tunnel, which was used for this investigation, is a single-return type with a rectangular test section. The

upper and lower walls are slotted longitudinally to allow continuous operation through the transonic speed range with negligible effects of choking and blockage. Stagnation pressures can be controlled from approximately 1/4 to 2 atmospheres with the tunnel stagnation temperature constant at 120° F. Design of the sting-support system is such that the model remains near the center line of the test section throughout the angle-of-attack range.

Models

Tests were performed with a 1.32-percent-scale model of the Saturn IB launch vehicle with various upper-stage configurations. Drawings of the models showing pertinent dimensions are shown in figure 1, and photographs showing three different combinations are presented in figures 2, 3, and 4. The models were fabricated basically of stainless steel and so designed that various components could be removed to facilitate the testing of various combinations. A description of each configuration is given in the following table:

TABLE I.- CONFIGURATIONS TESTED

Configuration	Flare angle	Fins	Shrouds	Launch escape system	Protuberances
1	8°37'	On	On	On	On
2	8°37'	Off	On	On	On
3	8°37'	On	On	Off	On
4	12°27'	On	On	On	On
5	8°37'	On	On	On	Off

Tests

Tests were conducted in the Langley 8-foot transonic pressure tunnel over a Mach number range from 0.50 to 1.20 and through angles of attack from -6° to 18°. Data were obtained only for configurations 1 and 2 at angles of sideslip from -4° to 10° at Mach numbers of 0.80 and 1.20. Data over the Mach number range were obtained with an internal six-component strain-gage balance at a stagnation pressure of 1 atmosphere, a stagnation temperature of 120° F, and at a dewpoint such that the results were free of condensation effects. Tests were conducted with natural transition and base pressures were measured with orifices located at the model base. The variation of test Reynolds number per foot with Mach number is shown in figure 5.

Corrections and Accuracy

Axial-force data presented herein are adjusted for the effects of model base pressure (correction includes shroud base area). A plot of the axial-force

correction is given in figure 6. The angles of attack and sideslip presented are corrected for model sting and balance deflection due to aerodynamic forces and moments on the model. An additional correction for tunnel airflow angularity has been applied to the angle of attack.

The effects of wind-tunnel boundary-reflected disturbances were negligible at all test Mach numbers.

The estimated accuracies of the data at a Mach number of 0.90 and a stagnation pressure of 1 atmosphere, based on instrument calibration and data repeatability, are within the following limits:

C_N . . . . ±0.034
C_A . . . . ±0.011
C_m . . . . ±0.090
C_l . . . . ±0.011
C_n . . . . ±0.045
C_Y . . . . ±0.023
M . . . . ±0.003

Model angles of attack are estimated to be accurate within ±0.1°.

RESULTS AND DISCUSSION

Presentation of Results

The results of this investigation are presented in the following figures:

Longitudinal Characteristics

Examination of the data in figures 7 and 11 indicates that the normal-force contribution of the fins was approximately 50 percent of the total normal force acting on the entire vehicle. These fin contributions are not reflected in the pitching-moment data (figs. 9 and 11) because of the particular choice of the moment reference center, which, as can be seen from figure 1, falls close to the fin center of area. Examination of figure 11 also shows that removal of the fins caused a forward shift of the centers of pressure of approximately 3 body diameters; however, the center-of-pressure variation with Mach number was less than 1 body diameter for all configurations tested.

Removal of the Apollo capsule and the launch escape tower to form the abort vehicle (configuration 3) had little effect on the normal-force and pitching-moment characteristics of the vehicle (figs. 7 and 9). The normal-force and pitching-moment results for the abort configuration (configuration 3) and the increased angle of the forward flare (configuration 4) are similar throughout the Mach number range (figs. 7 to 10). The effects of removing the protuberances from the second (S-IV-B) stage and increasing the angle of the forward flare on the normal-force and pitching-moment results were negligible in the lower angle-of-attack range ($\alpha = -6^{\circ}$ to 6°). However, at the higher angles of attack (figs. 8 and 10), it is interesting to note that removing the protuberances from the second (S-IV-B) stage (configuration 5) had a greater effect on the normal-force and pitching-moment characteristics, as compared with configuration 1, than did increasing the angle of the forward flare (configuration 4).

The data in figures 12, 13, and 14 show the transonic axial-force charac-teristics of the configurations tested; the abort configuration displayed the expected increase in axial force. The importance of base drag can be seen in figure 14 by noticing that the base axial-force coefficients vary from approx-imately 30 percent to 60 percent of the axial-force coefficients (uncorrected) for all configurations over the Mach number range.

6

Lateral Characteristics

Lateral characteristics for configurations 1 and 2 are presented in figures 15 to 18. A comparison of the lateral characteristics measured at an angle of attack of 0° with the longitudinal characteristics ($\beta = 0°$; and with a proper consideration of the sign conversion) indicates similar variations, as would be expected from the symmetry of the models.

CONCLUDING REMARKS

A wind-tunnel investigation has been conducted to determine the transonic aerodynamic characteristics of the Saturn IB-Apollo launch vehicle with interchangeable upper-stage configurations. The tests were conducted at Mach numbers from 0.50 to 1.20, angles of attack from -6° to 18°, and angles of sideslip from -4° to 10°.

The results of this investigation indicate that the normal-force contribution of the fins was approximately 50 percent of the total normal force acting on the entire vehicle. The abort configuration showed a substantial increase in axial force over the other configurations tested; however, the differences in the force and moment coefficients were generally small for all configurations. Also, removal of the protuberances from the second (S-IV-B) stage had a greater effect on the normal-force and pitching-moment characteristics, as compared with the basic configurations, than did increasing the angle of the forward flare.

Langley Research Center,
    National Aeronautics and Space Administration,
        Langley Station, Hampton, Va., March 9, 1965.

7
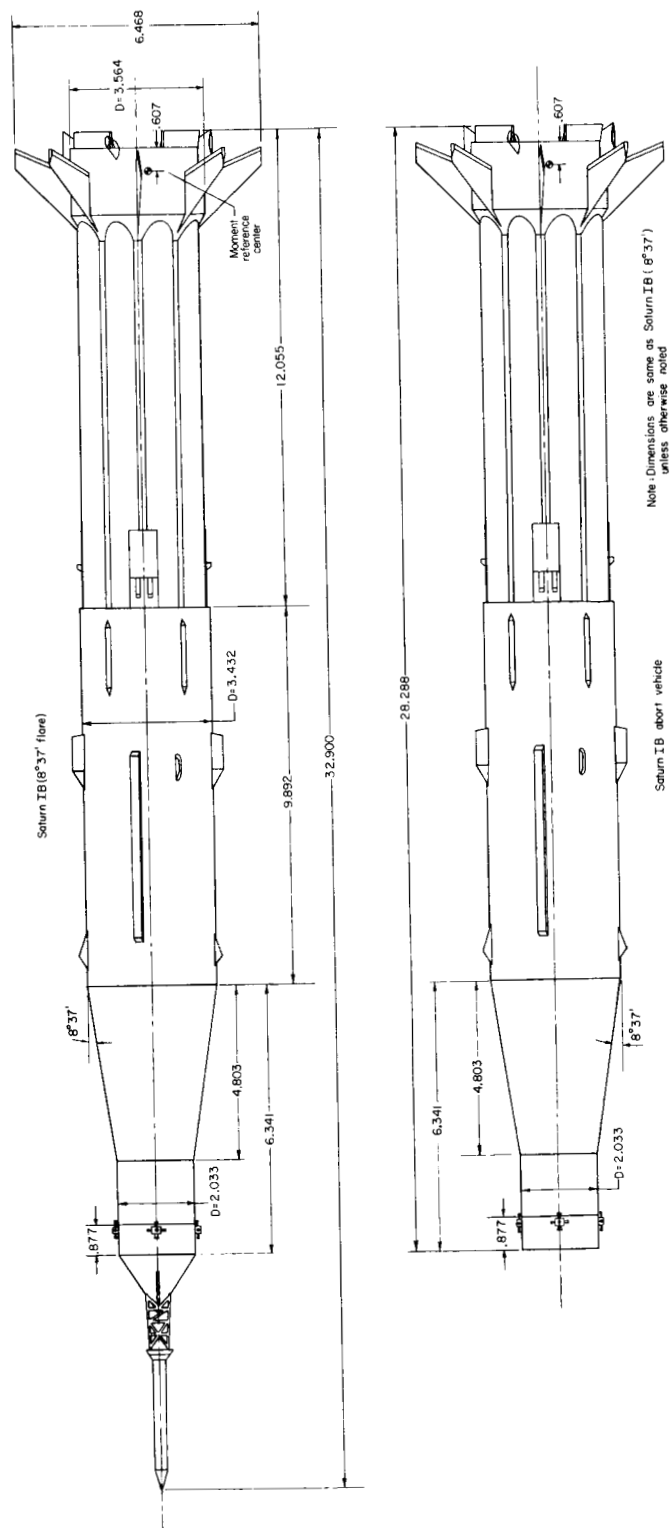
Figure 1.- Model geometrical details. All dimensions are in inches unless otherwise noted.
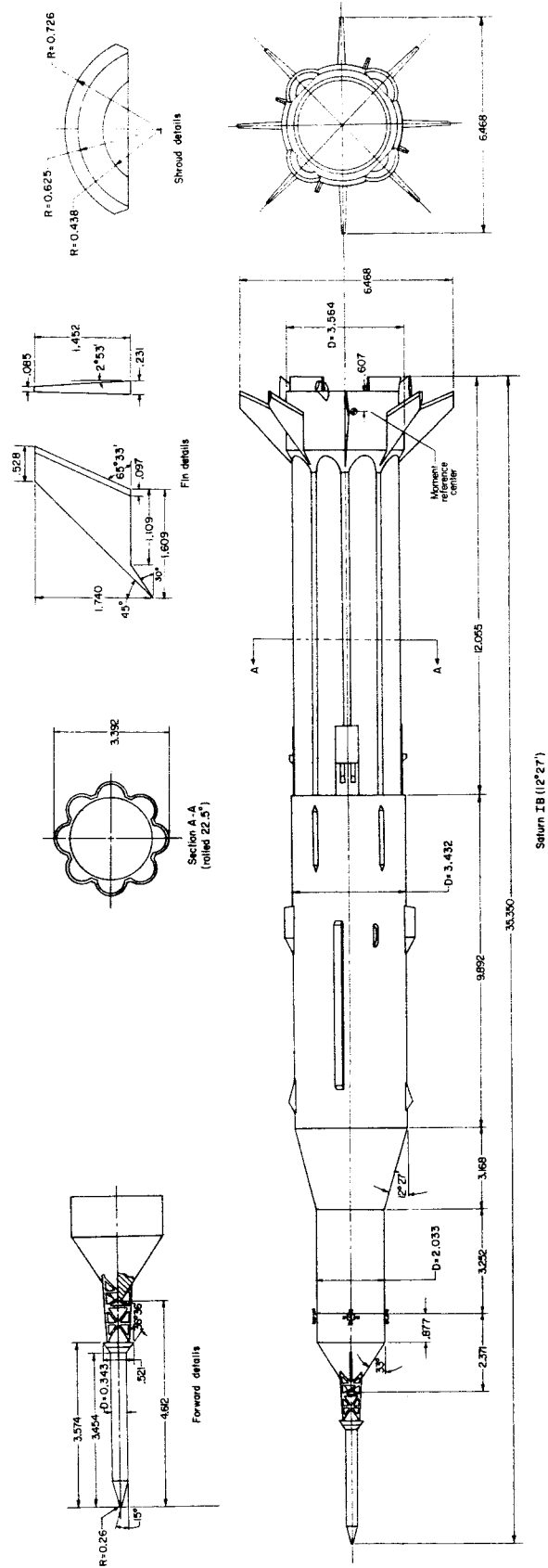
Figure 1.- Concluded.
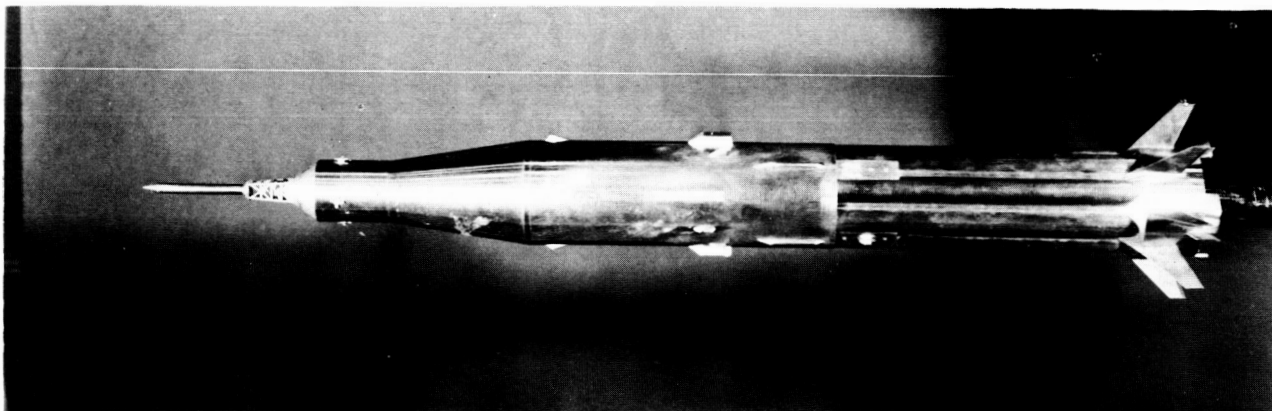
L-64-2705
Figure 2.- Photograph of Saturn IB-Apollo launch vehicle ($8^\circ 37'$ flare angle). First stage (S-IB) rolled counterclockwise 45° (as viewed from rear).
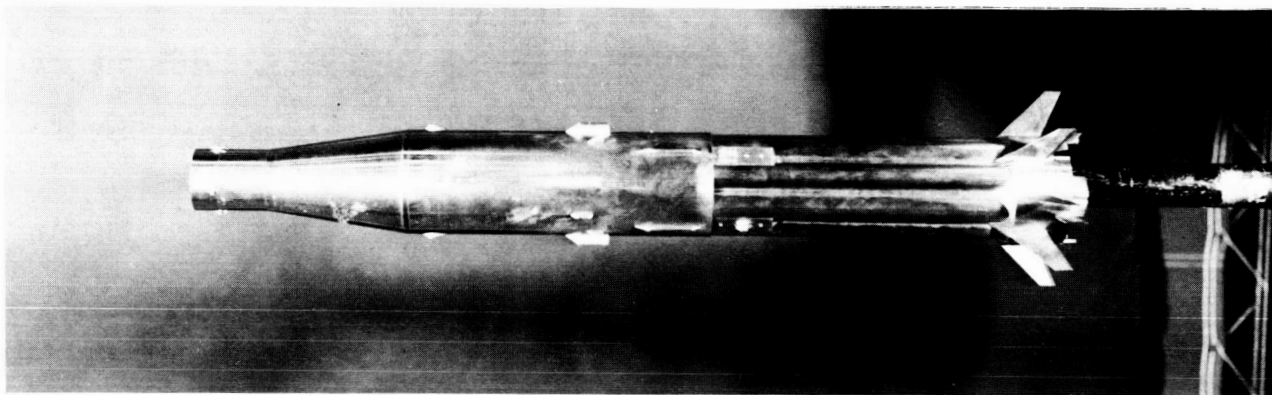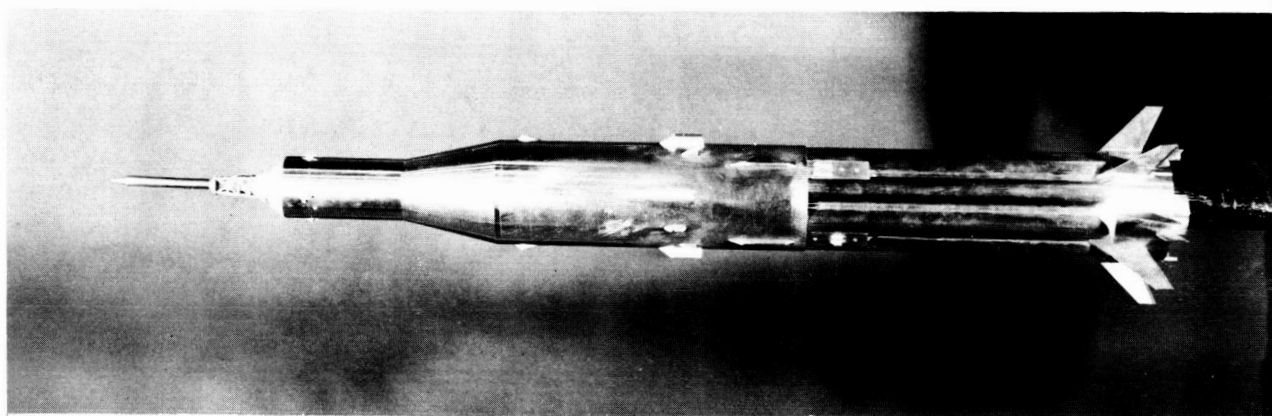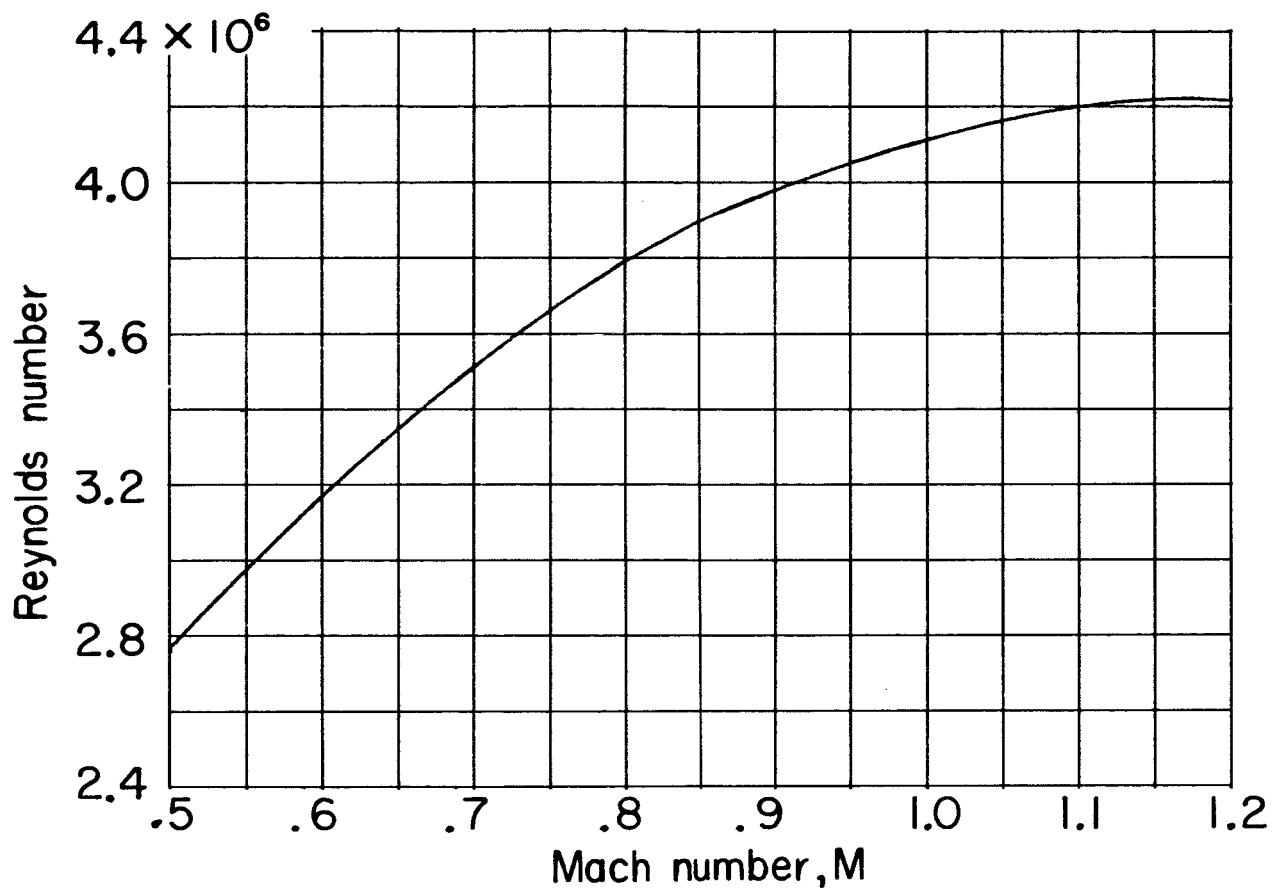

L-64-2707
Figure 3.- Photograph of Saturn IB-Apollo launch-abort vehicle ($8^\circ 37'$ flare angle). First stage (S-IB) rolled counterclockwise 45° (as viewed from rear).

L-64-2709
Figure 4.- Photograph of Saturn IB-Apollo launch vehicle ($12^\circ 27'$ flare angle). First stage (S-IB) rolled counterclockwise 45° (as viewed from rear).

10

Figure 5.- Variation of test Reynolds number per foot with Mach number.
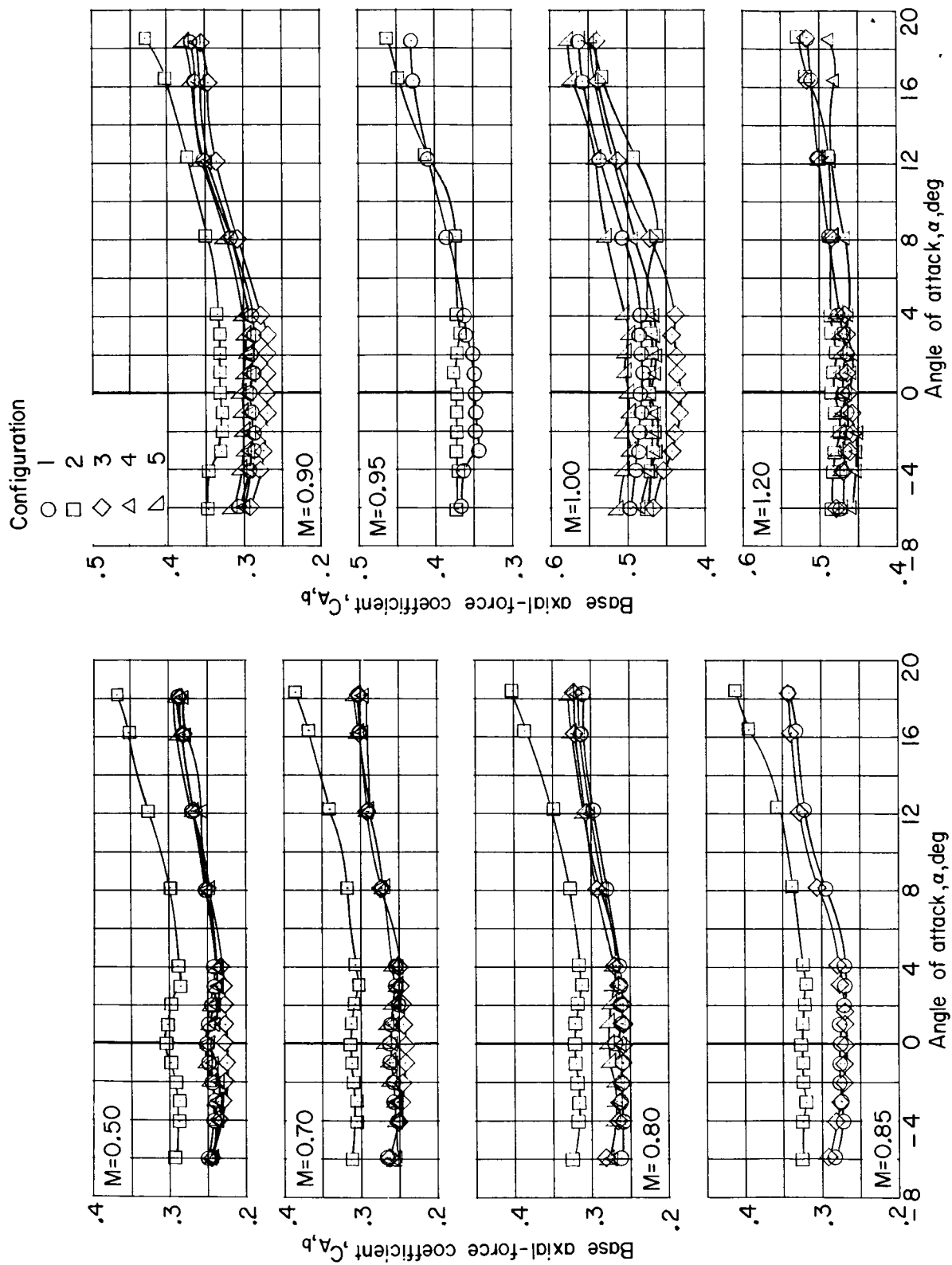
Figure 6.- Variation of axial-force correction with angle of attack for configurations 1, 2, 3, 4, and 5.
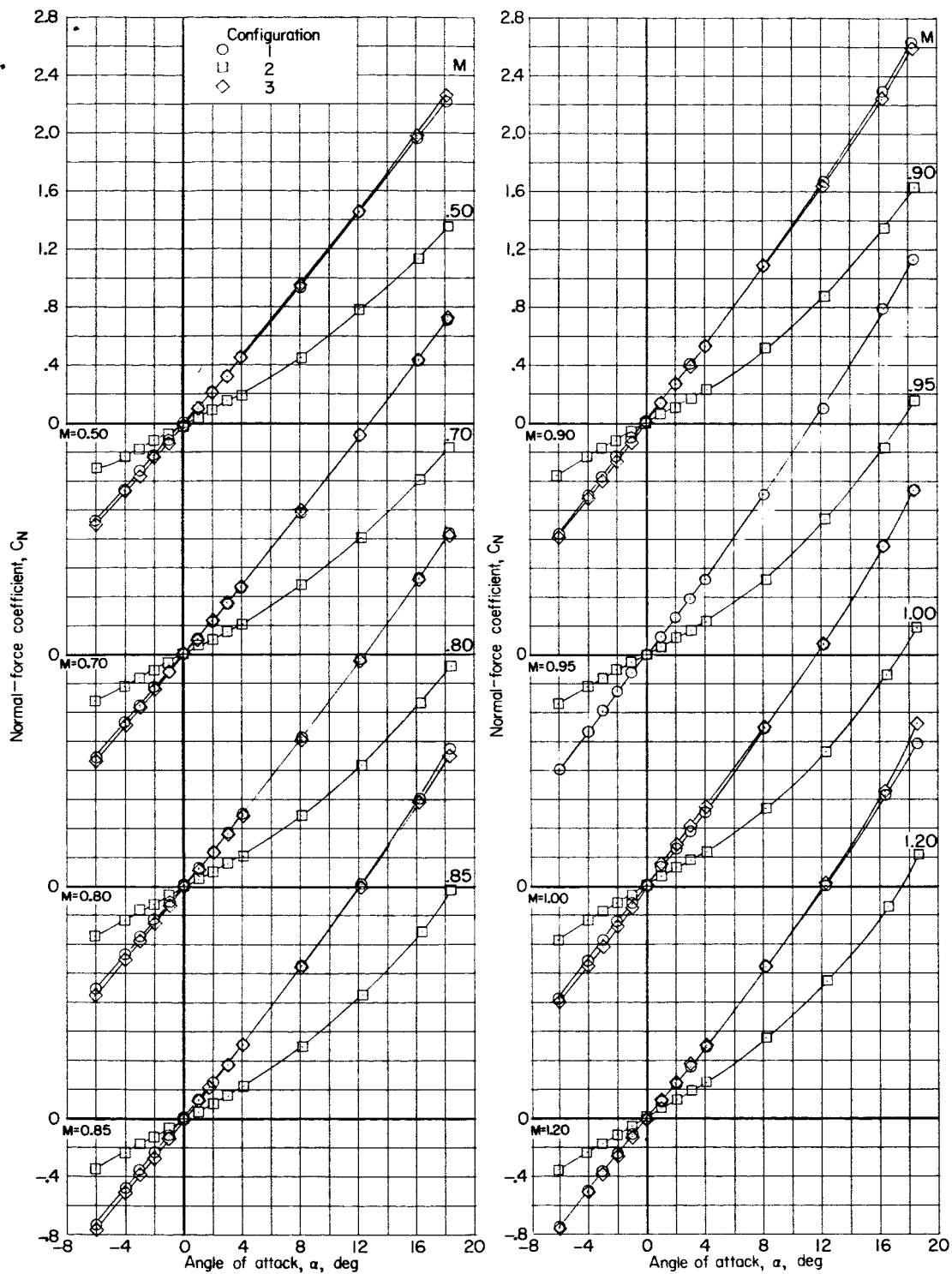
Figure 7.- Variation of normal-force coefficient with angle of attack for
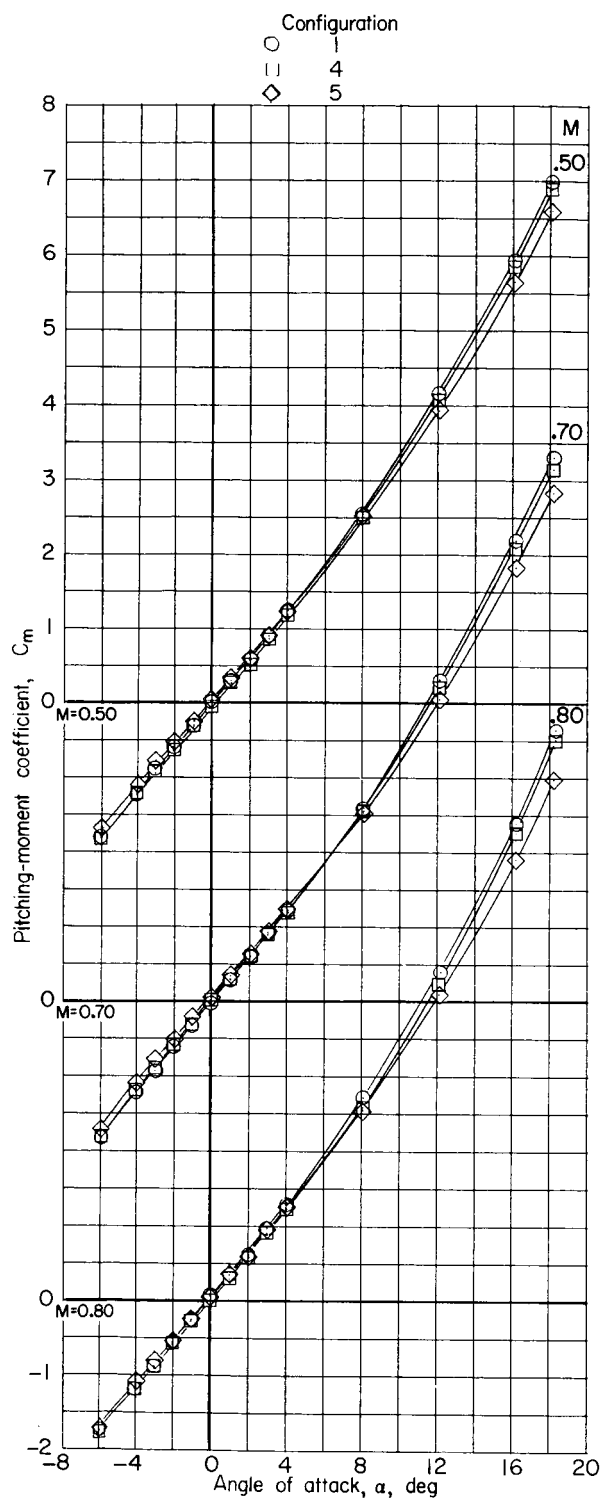configurations 1, 2, and 3.
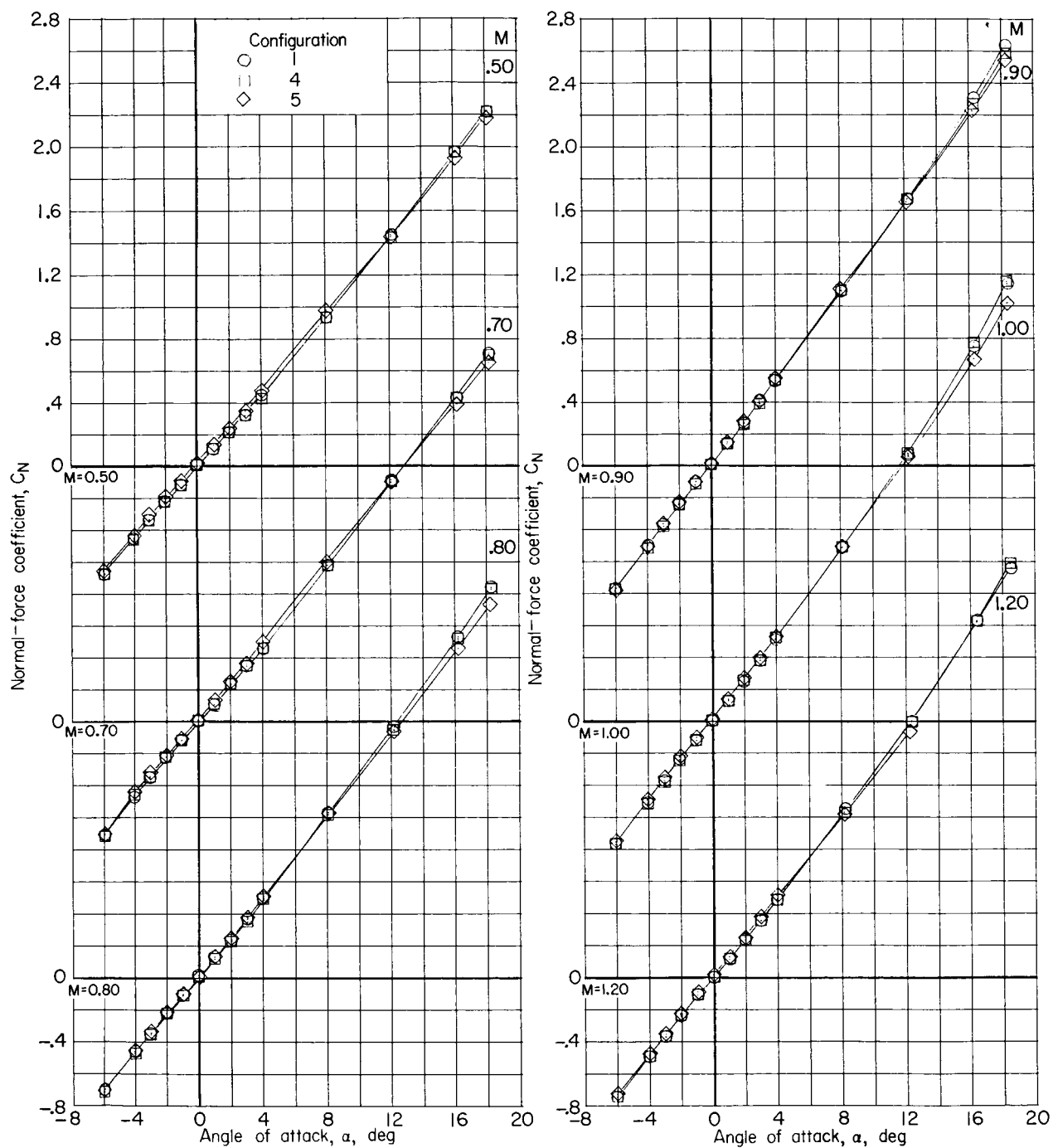
Figure 8.- Variation of normal-force coefficient with angle of attack for
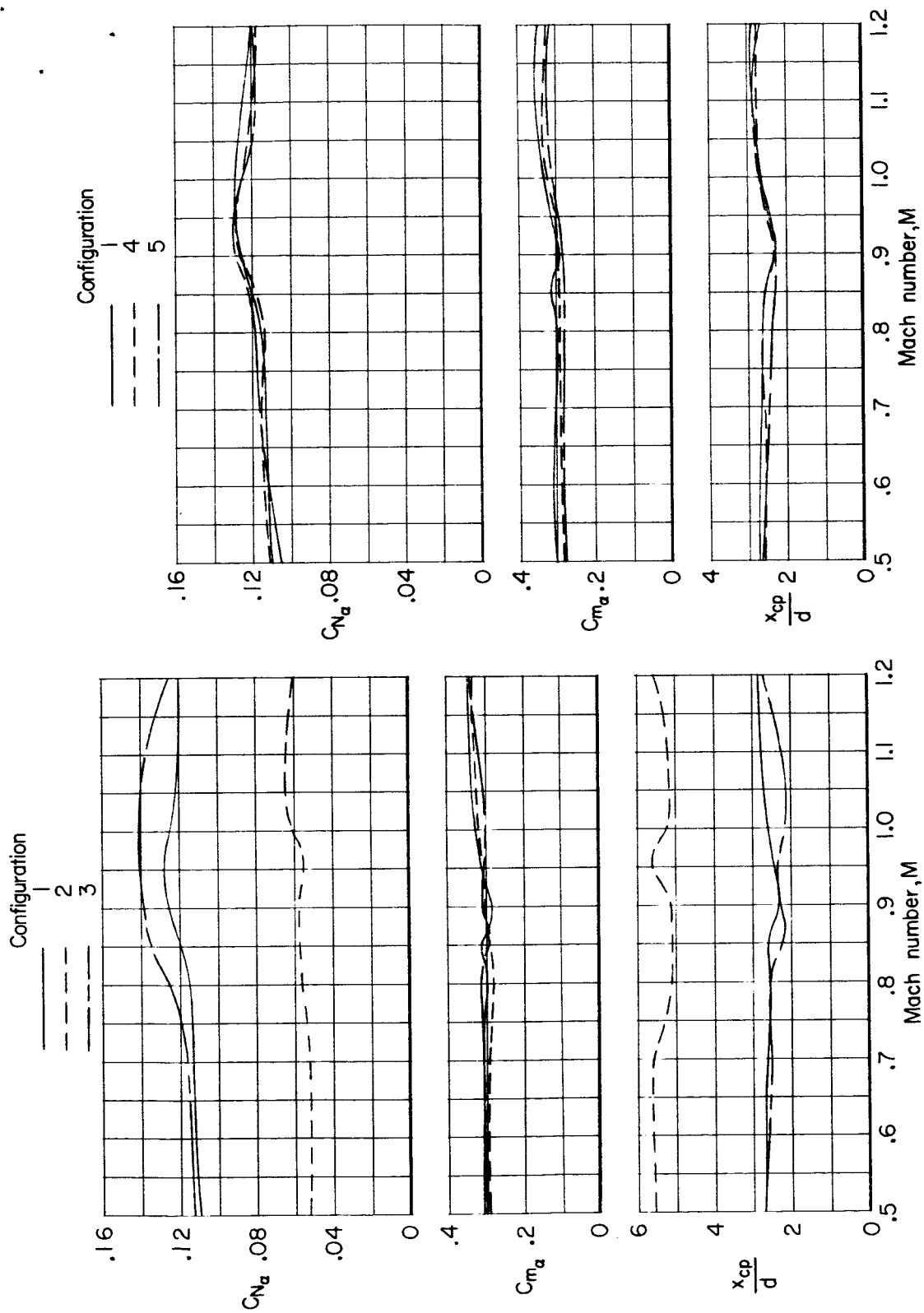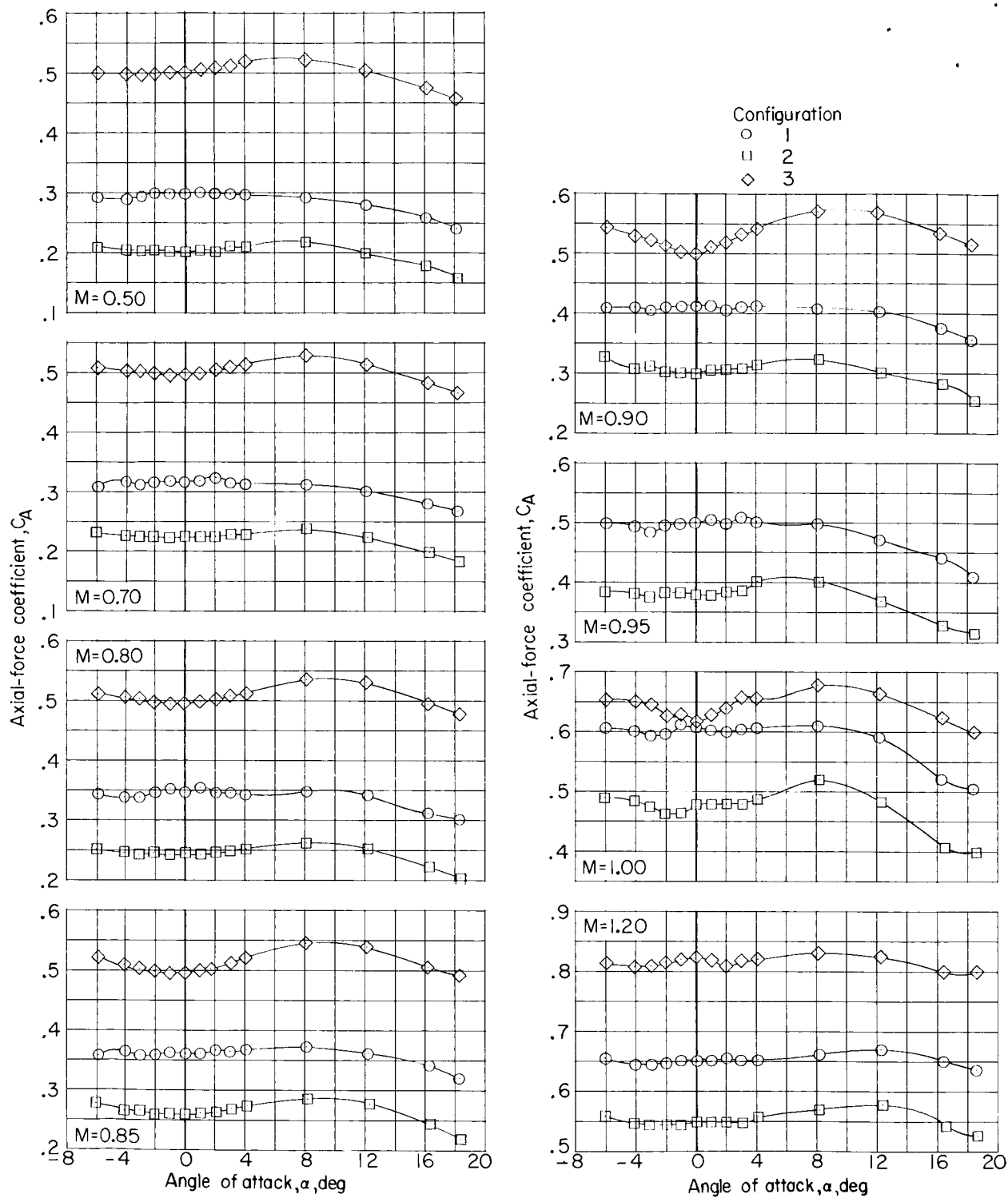configurations 1, 4, and 5.
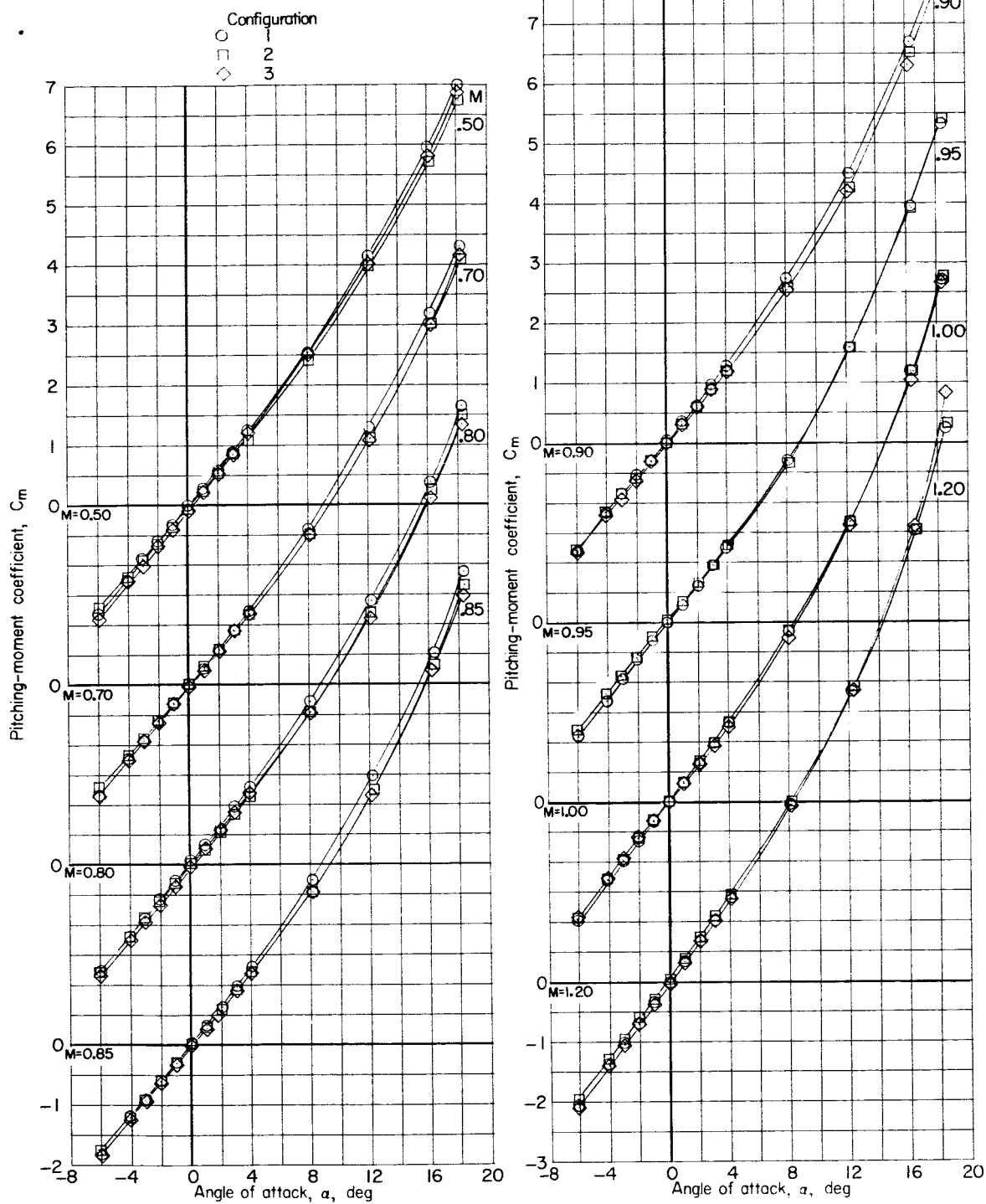
Figure 9.- Variation of pitching-moment coefficient with angle of attack for configurations 1, 2, and 3.
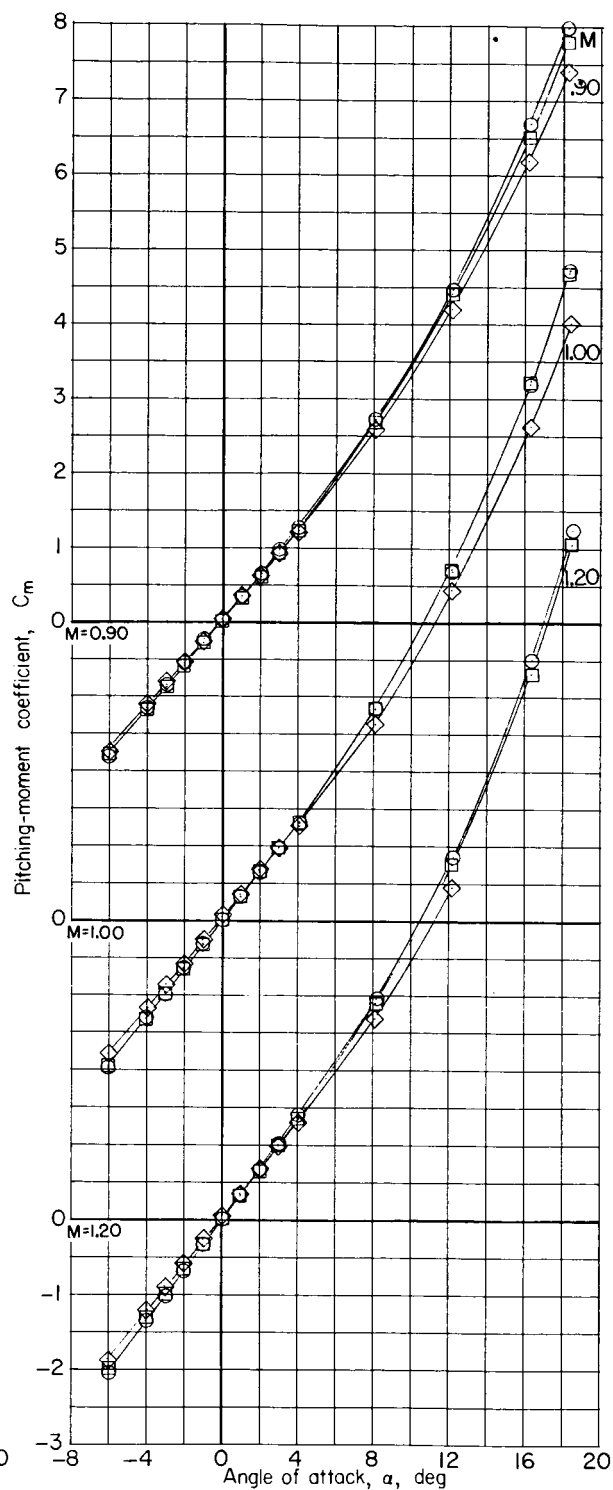
Figure 10.- Variation of pitching-moment coefficient with angle of attack for configurations 1, 4, and 5.

Figure 11.- Summary of longitudinal aerodynamic characteristics of configurations 1, 2, 3, 4, and 5 ($\alpha = 0°$).

Figure 12.- Variation of adjusted axial-force coefficients with angle of attack for configurations 1, 2, and 3.
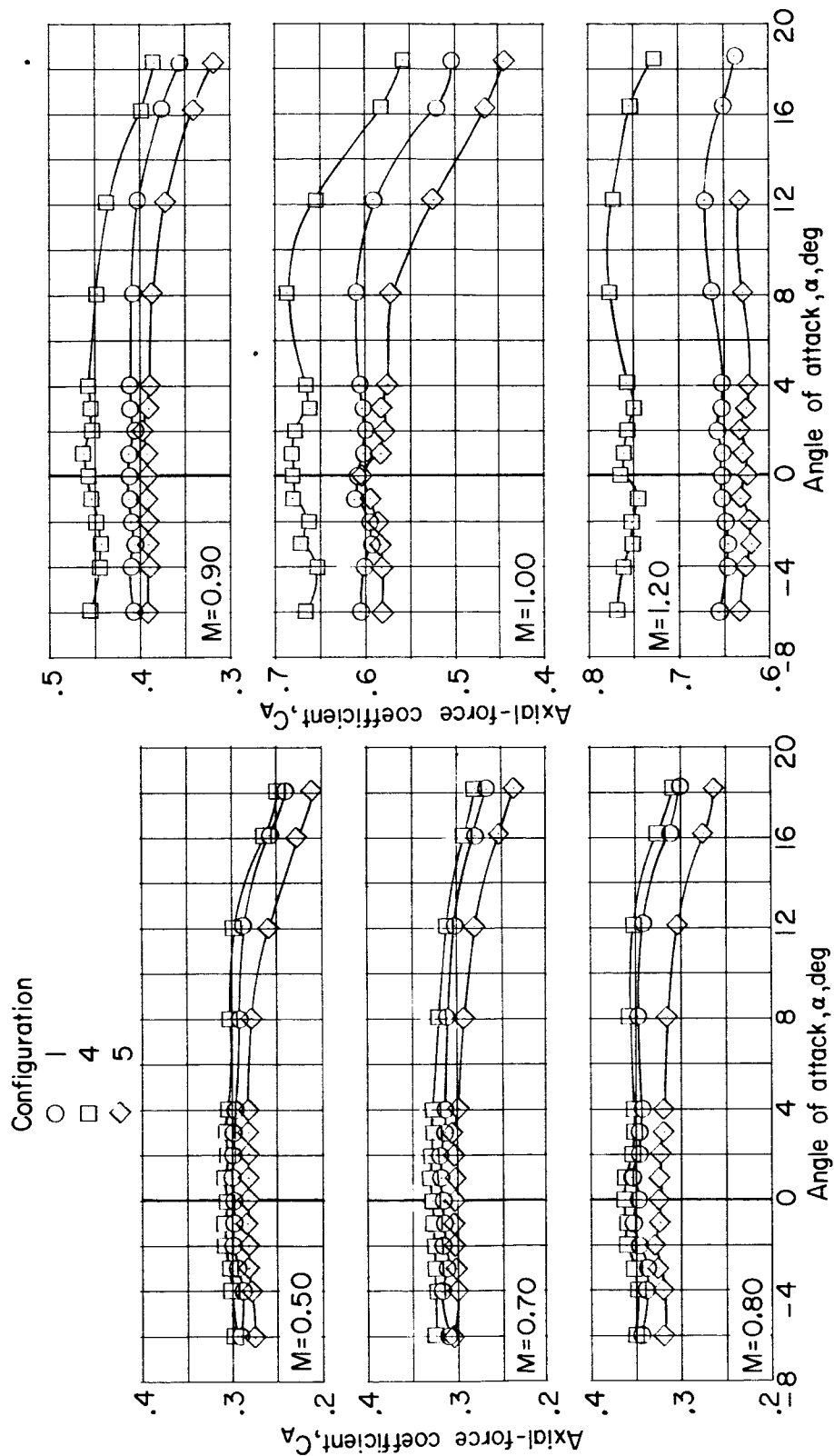
Figure 13.- Variation of adjusted axial-force coefficients with angle of attack for configurations 1, 4, and 5.
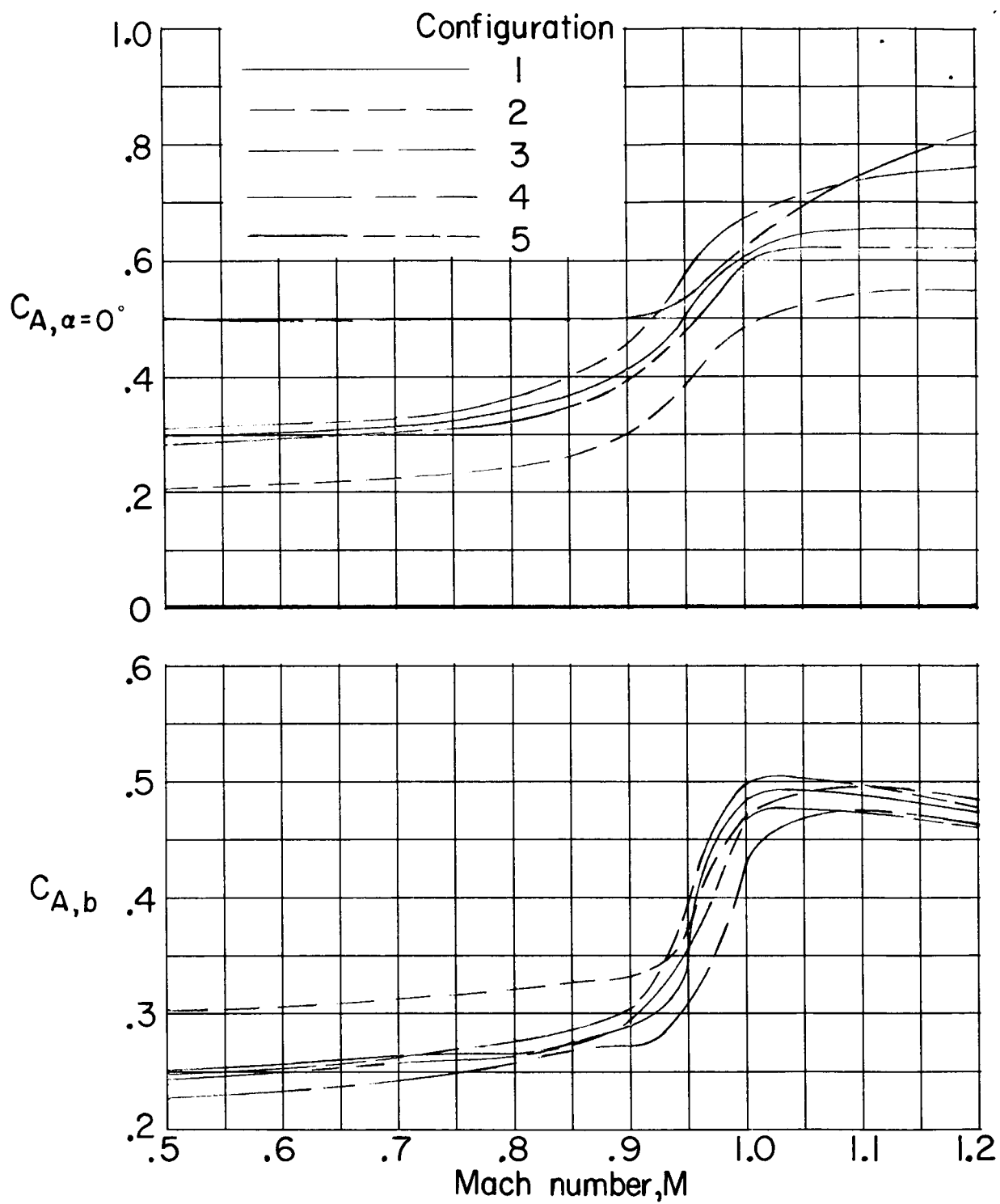
19

Figure 14.- Summary of transonic axial-force characteristics of configurations 1, 2, 3, 4, and 5.
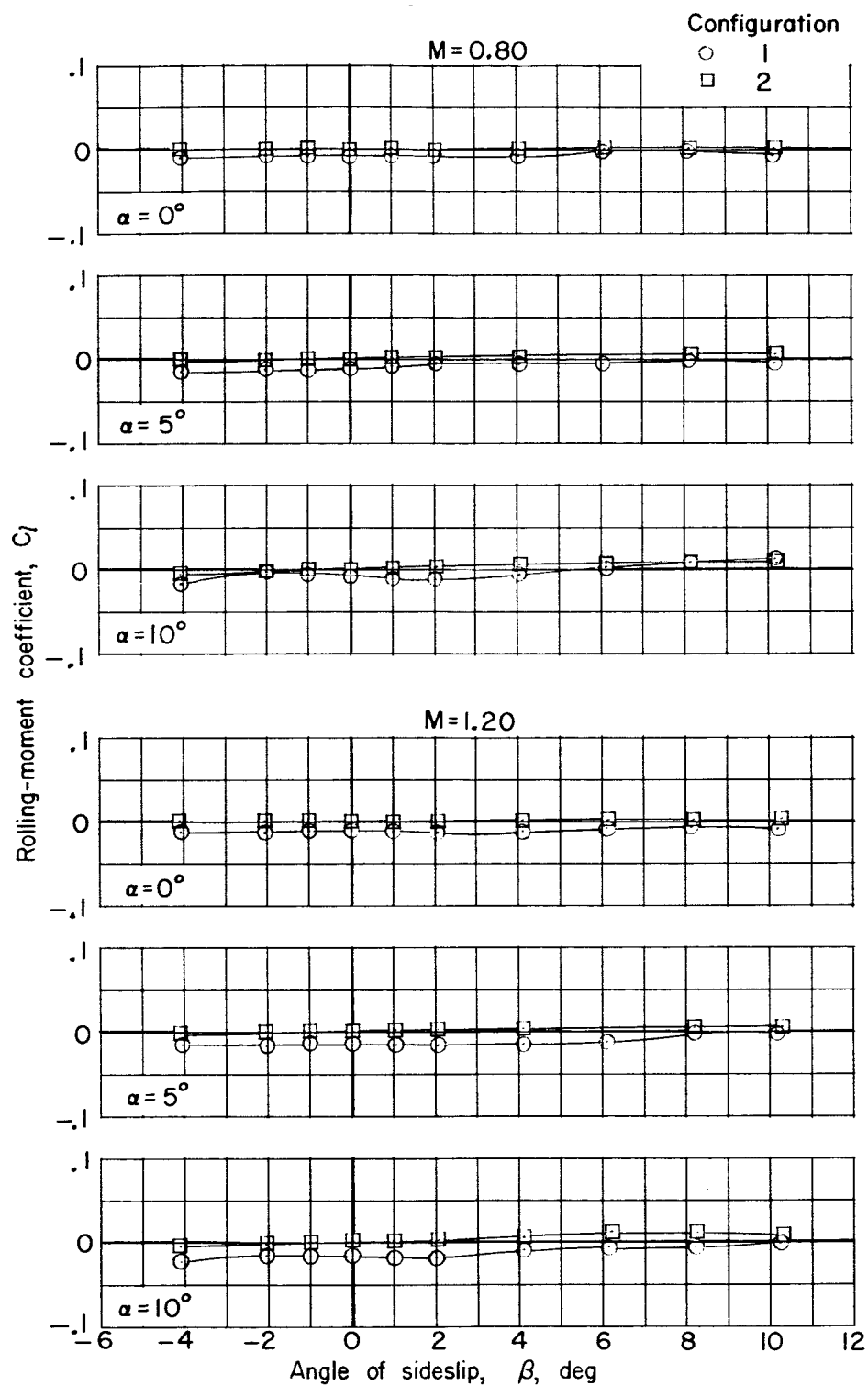
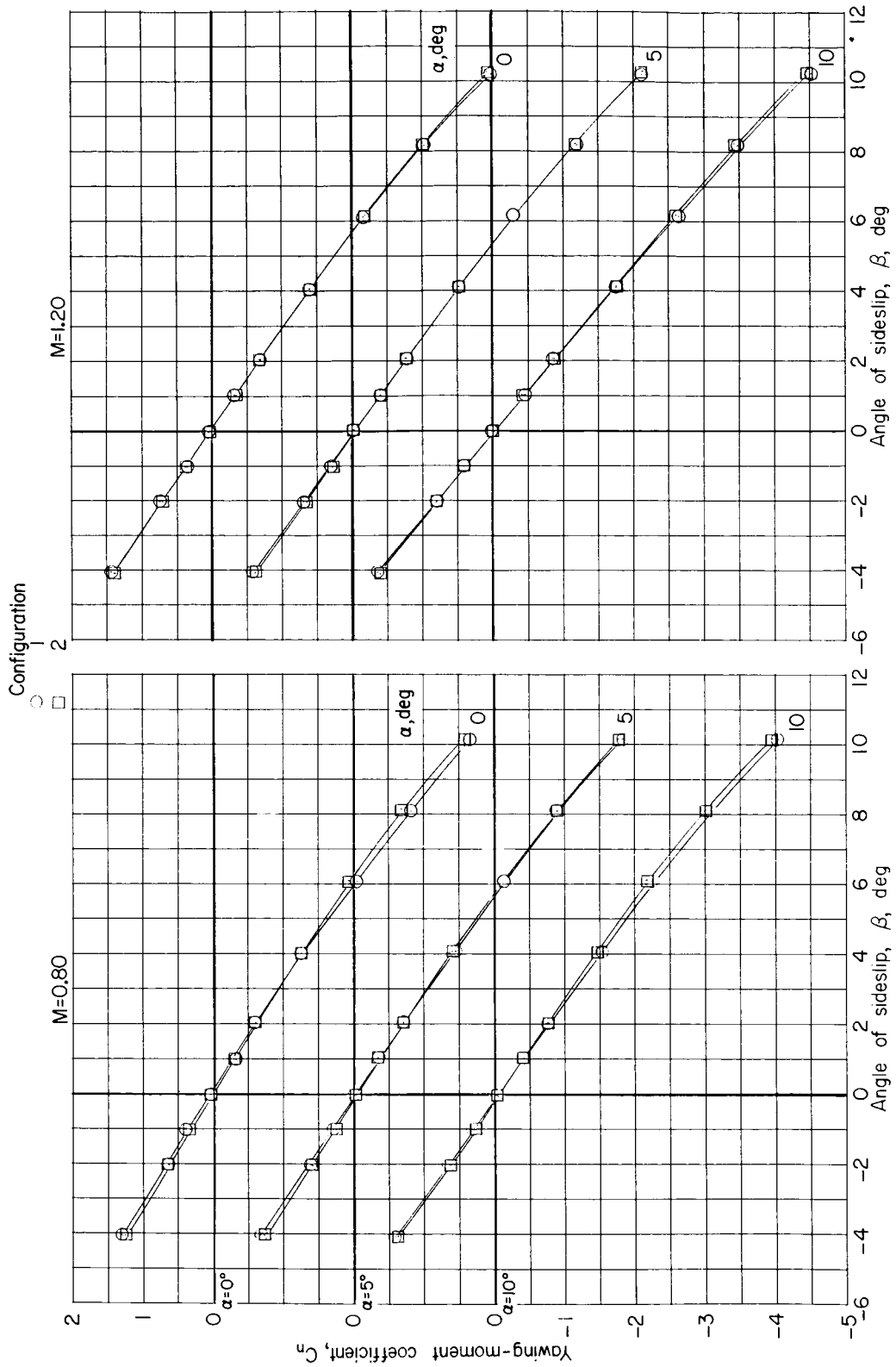Figure 15.- Variation of rolling-moment coefficient with angle of sideslip for configurations 1 and 2.

Figure 16.- Variation of yawing-moment coefficient with angle of sideslip for configurations 1 and 2.
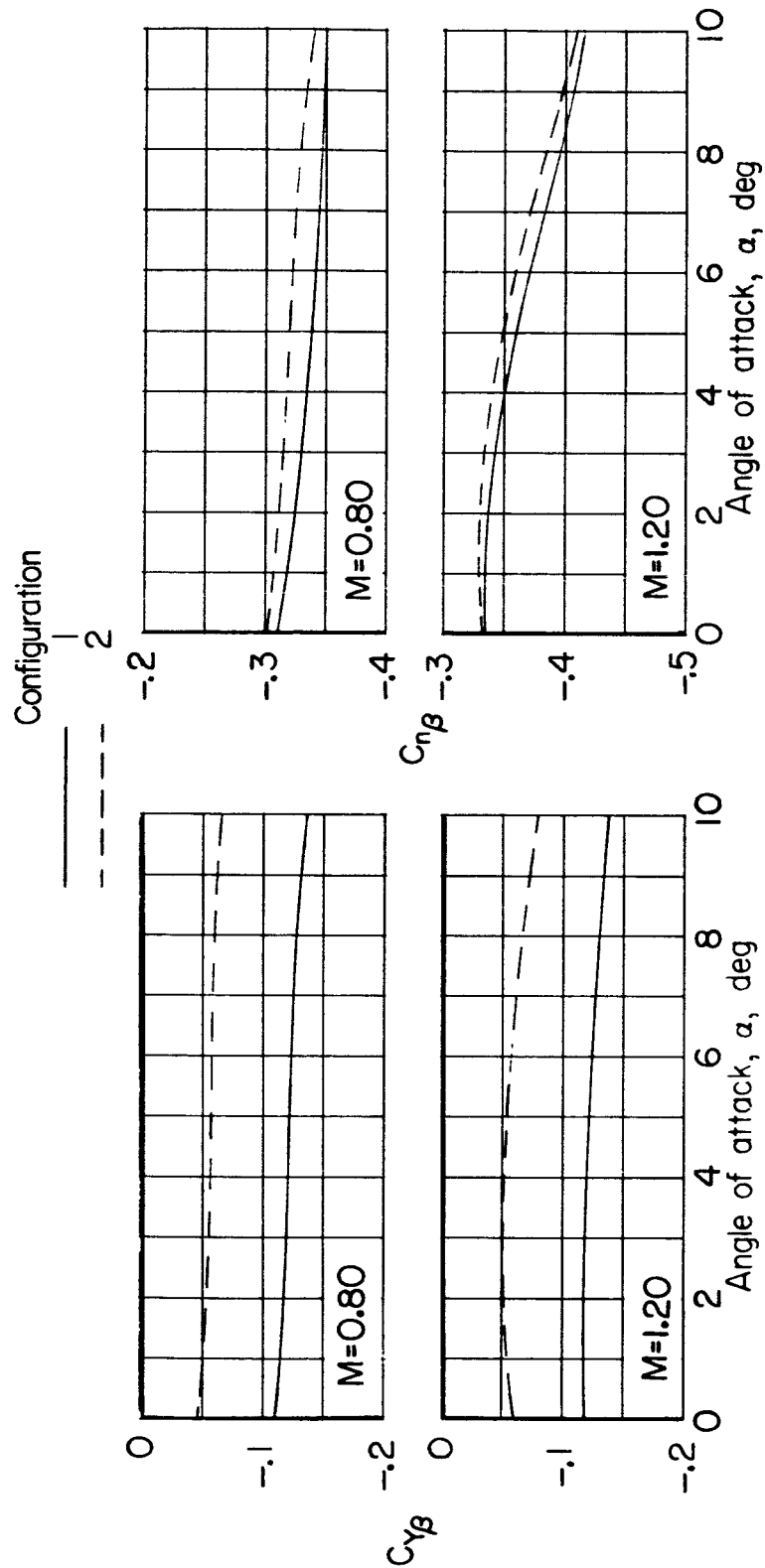
Figure 18.- Summary of lateral aerodynamic characteristics of configurations 1 and 2 ($\beta = 0^\circ$).
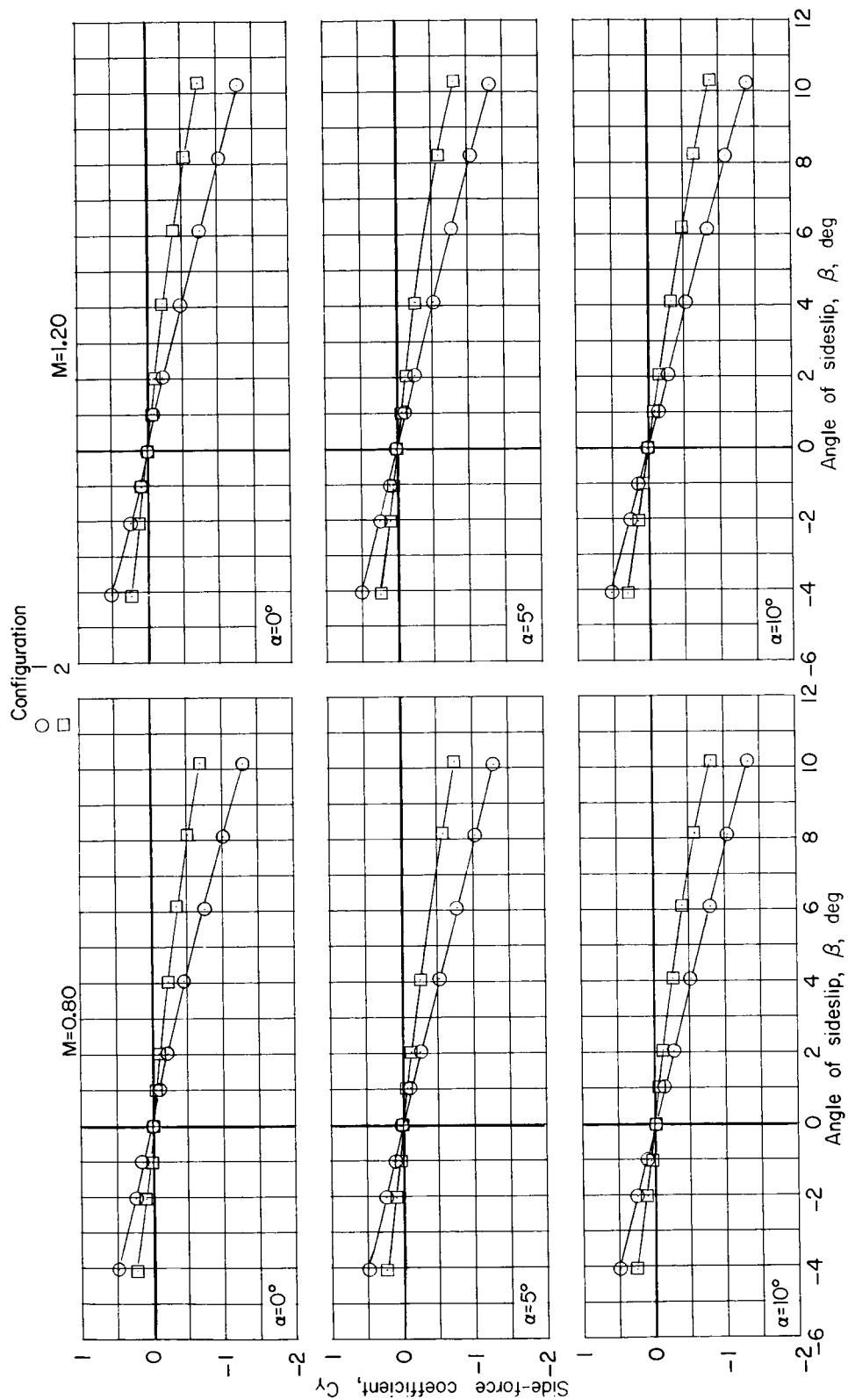
Figure 17.- Variation of side-force coefficient with angle of sideslip for configurations 1 and 2.